(tending to increase cloud coverage) through microphysical details of the aerosol population (specifically, their chemical composition and size distribution). Any net effect of these opposed tendencies depends on such microphysical details, as well as the meteorology. Rather than attempt to comprehensively evaluate any net effects, we instead decouple the forcings by varying the haze properties and cloud droplet concentrations separately.

24. The model domain is initially cloudless; the cited droplet concentrations apply only to grid cells in which clouds appear. In all simulations the number concentration of haze particles increases linearly from zero at the ocean surface up to 600 m, maintains a uniform value up to the trade inversion, and vanishes linearly in the overlying 300 m. The haze particle size distribution is log-normal with a geometric mean radius of 0.1 μm and a geometric SD of 1.8.
25. For clear-sky conditions at 5°N on March 1, a 1.8-km-deep layer of our idealized INDOEX 1998 haze absorbs 7.4 W/m^2 of solar radiation (diurnally averaged), which is comparable to the absorption measured during INDOEX 1998 (*10*). Optical properties of black carbon (soot) are taken from [P. Chylek, V. Ramaswamy, R. J. Cheng, *J. Atmos. Sci.* **41**, 3076 (1984)].
26. To address the sensitivity of the simulations to small variations in initial conditions, for the baseline we ran an ensemble of four simulations that differed only in the pseudo-random distribution of initial perturbations of temperature and water vapor. Output from one member of the ensemble is shown in Figs. 2 and 3.
27. Vertically resolved cloud fraction, defined as the fraction of cells in each layer with cloud water >0.05 g/kg, is distinct from the fractional cloud coverage we define subsequently, which is evaluated from vertically integrated columns.
28. During the first 5 days of ATEX (the observation period upon which our meteorology is based), surface reports of the cloud fractional coverage, which may include clouds above the boundary layer, ranged from an early morning maximum ~0.9 on two separate days to a minimum of ~0.2 one afternoon; the average value over the period was 0.5 [B. Albrecht, *J. Atmos. Sci.* **48**, 1519 (1991)]. For comparison, the simulated cloud coverage depends on a number of factors, including the criterion used to count cloudy grid columns, the model resolution, subgrid-scale mixing assumptions, and the water vapor above the inversion. With our model setup, the diurnal average (0.23) and range (0.1 to 0.4) from the baseline simulations are more comparable to those found over the Indian Ocean during the northeast monsoon (*11*).
29. We assume that all the enhanced solar absorption occurs only within the haze, though some fraction of the soot is likely to be incorporated into cloud droplets through nucleation and coagulation/coalescence. Cloud droplets (of typical radius 10 μm) collect significantly more sunlight than do haze (of typical radius 0.1 μm), and hence a fixed amount of soot will absorb more sunlight when embedded within cloud droplets (particularly when most of the haze lies below the bulk of cloud cover); such an effect could be expected to increase the impact of the soot on boundary-layer dynamics. Yet this expectation is not borne out by simulations in which all the soot is assumed to be within cloud droplets (when present within a grid cell) because such a small volume of boundary-layer air is occupied by cloud in our simulations.
30. "Cloud-burning" is the response of clouds to increased atmospheric heating, which includes reductions in cloud coverage and liquid and water path.
31. The reductions in cloud coverage due to solar absorption in the INDOEX hazes are not completely independent of droplet concentration. The strong increase in daytime cloud coverage between droplet concentrations of 50 and 100 cm^{-3} only for the simulations without soot implies that the effect of soot on cloud cover is maximum at a droplet concentration of 100 cm^{-3}. However, the departure of that maximum from the average cloud-burning effect is not significant compared to the noise found for the baseline ensemble.
32. As seen in Fig. 5B, the average liquid water path is roughly independent of droplet concentration for any particular aerosol. The increases of cloud coverage with droplet concentration in these simulations (Fig. 5A) are largely due to enhancement of total droplet cross-sectional area and therefore optical depth (which vary as the cube root of droplet concentration, holding liquid water path fixed). Because cloud coverage is defined as the fraction of columns exceeding an optical depth threshold (2.5), columns do not need as much liquid water path at increased droplet concentrations to be counted as cloudy.
33. Simulations with moisture enhanced above the inversion layer (at 6 g/kg, up from 4.5 g/kg used in our other simulations) produce moister clouds with greater fractional coverage that are more strongly influenced by both the soot cloud-burning and the conventional indirect aerosol effects.
34. An increase in cloud coverage results in more reflection of solar energy (a cooling effect), while at the same time allowing less infrared energy to escape to space (a warming effect). The solar forcing dominates any infrared compensation in trade cumulus, which therefore exert a net cooling influence (compare clear-sky to cloudy net fluxes in Fig. 5C).
35. J. T. Houghton *et al.*, *Climate Change 1995: The Science of Climate Change* (Cambridge Univ. Press, Cambridge, 1996), pp. 112–117.
36. S. K. Satheesh *et al.* [*J. Geophys. Res.* **104**, 27421 (1999)] estimate that 60% of the aerosol optical depth in the INDOEX 1998 haze was anthropogenic (accounting for an optical depth of 0.12 at 0.5 μm), which is 70% of the optical depth in our baseline haze.
37. The scope of our calculations (17 simulations of 30 hours) demand a number of computational efficiencies, which include parameterized cloud microphysics, moderate grid resolution and domain area, and no treatment of horizontal radiative transfer.
38. Y. J. Kaufman and R. S. Fraser, *Science* **277**, 1636 (1997).
39. Y. J. Kaufman and T. Nakajima, *J. Appl. Meteorol.* **32**, 729 (1993).
40. Distributed over a 2.5-km-deep boundary layer (not in a trade cumulus regime), the diurnal-average aerosol forcings reported by P. B. Russel *et al.* [*J. Geophys. Res.* **104**, 2289 (1999)] and P. Hignett, J. P. Taylor, P. N. Francis, M. D. Glew [*J. Geophys. Res.* **104**, 2279 (1999)] yield clear-sky heating rates of 0.5 and 0.6 K/day, respectively. In comparison, the diurnal-average aerosol-induced heating rates in the boundary layer range from 0.5 to 1 K/day for our idealized INDOEX hazes.
41. R. R. Draxler and G. D. Hess, *NOAA Tech. Memo. ERL ARL-224* (1997).
42. V. Manghani *et al.*, *Boundary-Layer Meteorol.*, in press.
43. E. J. Welton *et al.*, *Tellus B* **52**, 635 (2000).
44. Supported by NASA grants NAG5-6504 and NAG5-8362, the U.S. Department of Energy, and NSF. The Micro Pulse Lidar measurements were supported by NASA contract NA55-31363 and the NASA SIMBIOS project. We thank J. Coakley for performing radiative transfer calculations for comparison against ours, C. Twohy for helpful discussions regarding droplet nuclei measurements from INDOEX, the NOAA Pacific Marine Environmental Laboratory (PMEL) and the crews of the R/V *Ronald H. Brown* and the National Center for Atmospheric Research (NCAR) C-130 aircraft for making the INDOEX measurements possible, and two anonymous reviewers for comments that improved the manuscript.

15 December 1999; accepted 29 March 2000

N-Cadherin, a Cell Adhesion Molecule Involved in Establishment of Embryonic Left-Right Asymmetry

Martín I. García-Castro,*† Eva Vielmetter,* Marianne Bronner-Fraser

Within the bilaterally symmetric vertebrate body plan, many organs develop asymmetrically. Here, it is demonstrated that a cell adhesion molecule, N-cadherin, is one of the earliest proteins to be asymmetrically expressed in the chicken embryo and that its activity is required during gastrulation for proper establishment of the left-right axis. Blocking N-cadherin function randomizes heart looping and alters the expression of Snail and Pitx2, later components of the molecular cascade that regulate left-right asymmetry. However, the expression of other components of this cascade (Nodal and Lefty) was unchanged after blocking N-cadherin function, suggesting the existence of parallel pathways in the establishment of left-right morphogenesis. Here, the results suggest that N-cadherin-mediated cell adhesion events are required for establishment of left-right asymmetry.

Several organs of the vertebrate body, such as the heart, lungs, liver, and gut, develop asymmetrically. For example, the initially symmetric heart tube loops to the right before it forms the multichambered heart [reviewed in (*1*)]. In the chicken, the earliest morphological sign of embryonic asymmetry appears during gastrulation in the chicken organizer, known as Hensen's node (*2*). Although it is initially symmetric, the anterior right portion of the node protrudes to the right by stage 4+ (*3–6*).

Early molecular markers define a pathway that mediates signaling of left-right asymmetry in the vertebrate embryo [reviewed in (*7–11*)]. Signaling in the node of the gastru-

Division of Biology 139-74, California Institute of Technology, Pasadena, CA 91125, USA.

*These authors contributed equally to this work.
†To whom correspondence should be addressed. E-mail: mig1000@caltech.edu

lating embryo in turn affects asymmetric expression of genes in the lateral plate mesoderm and asymmetric morphogenesis. In the chicken embryo, this process seems to be initiated by tissue surrounding the node (*12*). An activin-mediated signal on the right side of the node is thought to limit the originally symmetric expression of Shh to the left and induce the expression of FGF8 on the right (*13*, *14*). This subsequently leads to asymmetric expression in the lateral plate mesoderm of the secreted molecules Nodal, Lefty, and Caronte (*15*, *16*) and the transcription factors Snail and Pitx2 (*17*–*21*), which in turn leads to divergent left-right morphogenesis. Several of these components participate in left-right asymmetry in other vertebrate systems; however, their location and interactions vary (*22*).

These molecular signals direct mechanical components that generate this asymmetry. In the mouse, cilia in the node may play a role in asymmetrically distributing essential factors (*23*, *24*) and gap junctions may regulate flow of information that is important for left-right asymmetry (*25, 26*). It is likely that molecules governing cell adhesion or migration also direct asymmetry. Here, we show that the calcium-dependent cell adhesion molecule N-cadherin (*27*, *28*) has the appropriate spatiotemporal distribution to be involved in generating left-right asymmetry and that inhibiting its function perturbs this process.

We examined the distribution of N-cadherin transcripts by whole-mount in situ hybridization (*29*) of gastrulating chicken embryos ranging from Hamburger and Hamilton stages 3 to 6 (*30*). In stage 3 embryos, as the primitive streak elongates, N-cadherin expression appears to be symmetric within the streak (Fig. 1A). By stage 3+ to 4, when the primitive streak reaches its full length, levels of N-cadherin transcript are more abundant on the left side of the primitive streak (Fig. 1B). As Hensen's node appears and starts to regress (stage 4+ to 5; Fig. 1E), N-cadherin is expressed asymmetrically within the node itself (Fig. 1C) and is most prominent on the right anterior border of the primitive pit (Fig. 1D). In addition, there is a crescent of staining on the left posterior margin, which appears to be continuous with the anterior-most part of the left primitive fold. The streak maintains left-sided asymmetric expression of N-cadherin between stages 4− and 5 (Fig. 1, C and D). The expression pattern of N-cadherin partially overlaps with that of ActRIIa on the anterior right side of the node but not in the primitive streak (Fig. 1F). In the node of stage 4 embryos, N-cadherin is absent from Shh-expressing regions (Fig. 1G, anterior left). However, stage 4 embryos that display symmetric expression of Shh already show asymmetric expression of N-cadherin (Fig. 1G, inset). Therefore, N-cadherin asymmetry appears after that of ActRIIa and slightly before that of Shh.

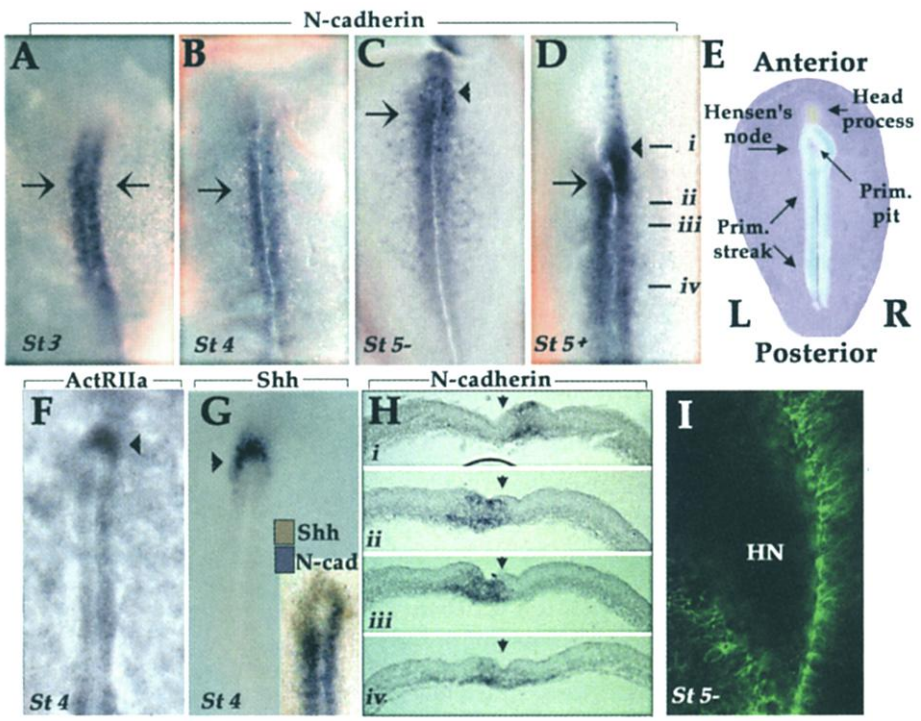

Fig. 1. Expression pattern of N-cadherin during early chicken development (HH stage 3 to 5). All views of embryos are dorsal except in (H); anterior is at the top, posterior is at the bottom. In situ hybridization patterns are shown for N-cadherin (A to D, and H), ActRIIa (F), and Shh (G) and were performed as described (*29*). (A to D, F, and G) Arrows point to high-expression areas on the primitive streak, and arrowheads point to high-expression areas in the node. (**A** to **D**) N-Cadherin expression in a progression from stage 3 to 5+. At Hamburger and Hamilton stage 3 (A), N-cadherin is symmetrically distributed in the primitive streak. From stage 4 to 5+ (B to D), N-cadherin expression is more intense on the left primitive fold. As the head mesoderm is laid down, the node becomes asymmetric and N-cadherin is expressed on the anterior right and posterior left margins of the node (C). Asymmetric distribution of N-cadherin is seen both in the node [anterior right (arrowheads), posterior left] and in the primitive streak [intense staining in the left primitive fold (arrows)]. (**E**) Colorized image of a stage 5− embryo showing the primitive (Prim) streak, Hensen's node, primitive pit, and head mesoderm. (**F**) ActRIIa expression at stage 4. (**G**) Shh expression at stage 4; inlay inset shows double in situ hybridization for N-cadherin (blue) and Shh (brown) at stage 4−; N-cadherin asymmetric expression overlaps with the symmetric expression of Shh on the right side of the node. (**H**) Transverse sections through regions corresponding to the labeled bars of an embryo similar to that shown in (C). Central axis of the embryo is indicated by the arrowhead. (i) In a mid-anterior region of the node, N-cadherin expression can be seen on the right side of the central axis of the embryo. In contrast, more caudal sections 60 (ii), 90 (iii), and 210 (iv) μm away from (i) display clear left-sided staining in all three tissue layers. (**I**) Confocal image showing N-cadherin protein detected by fluorescent immunohistochemistry (NCD2 antibody) in Hensen's node at stage 4+.

The mesoderm cells lateral to the primitive streak of stage 4 and older embryos form lateral plate mesoderm, which contains many of the late molecular markers involved in left-right morphogenesis and also part of the heart (*31*–*36*). Therefore, N-cadherin has a spatiotemporal distribution consistent with a role in initiating left-right asymmetry as well as a later role in heart development.

To test the role of N-cadherin in the establishment of left-right asymmetry, we blocked its function with monoclonal antibody NCD-2, which specifically binds to and inactivates N-cadherin (*28*). Gastrulating

chicken embryos (stage 3 to 4) were placed into New culture (*37*) in the presence of N-cadherin function-blocking antibody or a control antibody and grown for 24 to 36 hours. To examine whether N-cadherin function is essential for normal left-right morphogenesis, we used the direction of heart looping as a morphological marker for left-right asymmetry. In New culture, embryos complete gastrulation and neurulation, developing from 10 to 16 somite pairs. Only those embryos that displayed recognizable heart tube features were scored. In stage 3 to 4 embryos treated with control antibody, the tubular heart looped to the right, which is normal in most cases; only 8% looped to the left (n = 25) (Fig. 2) (Table 1). In contrast, in 41% of stage 3 to 4 embryos treated with anti-N-cadherin, the heart looped to the left (n = 58) (Fig. 2) (Table 1), which is consistent with a randomization of left-right morphogenesis. Although most embryos were removed from culture for analysis at early stages, four embryos treated with anti-N-cadherin at stage 3 to 4 developed sufficient to display head and anterior trunk rotation. In all these embryos, not only the heart but also the direction of rotation of the head and body axis were inverted. Treatment of embryos at stage 3 to 4 with a 1:10 dilution of anti-N-cadherin resulted in a proportional reduction in effect (14%) (n = 7); lower dilutions had no effect (n = 4). The normal direction of heart looping observed in embryos treated with control antibody as well as the proportional reduction in randomization after serial dilution suggest that the effects of anti-N-cadherin are specific and affect left-right asymmetry.

To determine the time period when N-cadherin affects left-right asymmetry, we treated embryos with anti-N-cadherin at older stages (Table 1). Only 18% of embryos treated at stage 5 had leftward heart looping (n = 16), whereas treatment at stage 6 had no effect on the direction of looping (n = 14). These results suggest that N-cadherin affects the direction of heart looping only during the period when it is asymmetrically expressed in Hensen's node and the primitive streak. Others have shown alterations in heart formation, but no effects on heart looping, when N-cadherin activity was blocked after stage 5 (*38*).

Activin- and Shh-mediated signals modify the expression of several components of the left-right pathway and alter left-right morphogenesis (*13*). To test whether these factors can also modify N-cadherin expression, we implanted beads coated with activin, Shh, or bovine serum albumin (BSA) adjacent to Hensen's node at stage 3+. Embryos were grown in New culture and collected after 6 to 9 hours. Because the beads themselves can interfere with development, only those embryos with recognizable nodes, head folds, and primitive streaks were analyzed further. After placement of activin-coated beads on the left side, complementary to the normal expression of ActRIIa on the right, 40% of the embryos exhibited altered patterns of N-cadherin distribution (n = 6/16). Five embryos (31%) displayed a mirror-image inversion of the normal N-cadherin expression pattern (Fig. 3B) as well as inversion of the node itself. In contrast, most (86%) embryos treated with control BSA-coated beads (n = 18/21) were normal. Shh-coated beads placed on the right, complementary to the normal distribution of Shh on the left, altered the pattern of N-cadherin expression in 60% of the embryos (n = 18/30). Defects included inversions of the expression pattern of N-cadherin [26% of embryos (n = 8/30)] similar to those observed with activin-coated beads and symmetric N-cadherin expression [20% of embryos (6/30)] (Fig. 3C). In addition, some embryos displayed inhibition of endogenous N-cadherin expression or its induction in ectopic regions. In contrast, treatment with BSA-coated beads resulted in normal N-cadherin expression in most cases (n = 20/24) (Fig. 3A). Thus, N-cadherin expression can be regulated directly or indirectly by signals implicated in establishment of left-right asymmetry. The early symmetric expression of Shh in the node could set the stage for subsequent asymmetric N-cadherin expression and/or asymmetric expression of Shh may maintain that of N-cadherin.

The normal direction of heart looping depends on expression of a number of signals from the lateral plate mesoderm, which are downstream of ActRIIa and Shh. Most notably, Nodal, Caronte, Lefty, and Pitx2 are expressed on the left side of the chicken embryo, and FGF8 and Snail are expressed on the right (*13–15*, *17*, *19–21*). To investigate the role of N-cadherin in establishing the asymmetric distribution of these genes, we examined their expression in stage 3 to 4 embryos cultured in the presence of function-blocking anti-N-cadherin for 6 to 12 hours (ActRIIa, Shh, and FGF-8) or for 12-24 hours (Nodal, lefty, Snail, and Pitx2). The distribution patterns of the early markers ActRIIa (n = 8), Shh (n = 28), and FGF8 (n = 19) were unchanged relative to age-matched controls (n = 6, 13, and 20, respectively), whereas patterns of later markers were differentially affected.

After blocking N-cadherin function at stage 3 to 4, Snail expression, which is normally stronger in the right lateral plate mesoderm, was altered in 30% of embryos (n = 13) (Fig. 4, C and D). Of these, two embryos had symmetric Snail expression and two others had inverted asymmetry, with stronger expression in the left lateral plate mesoderm. Control embryos showed no alterations in Snail expression (n = 13) (Fig. 4, A and B). Expression of Pitx2, which normally marks the left lateral plate mesoderm and the left side of the fusing heart tube was modified in 40% of the embryos treated with anti-N-cadherin (n = 15). Some embryos displayed bilateral expression of Pitx2 (Fig. 4, G and H), whereas others displayed stronger expres-

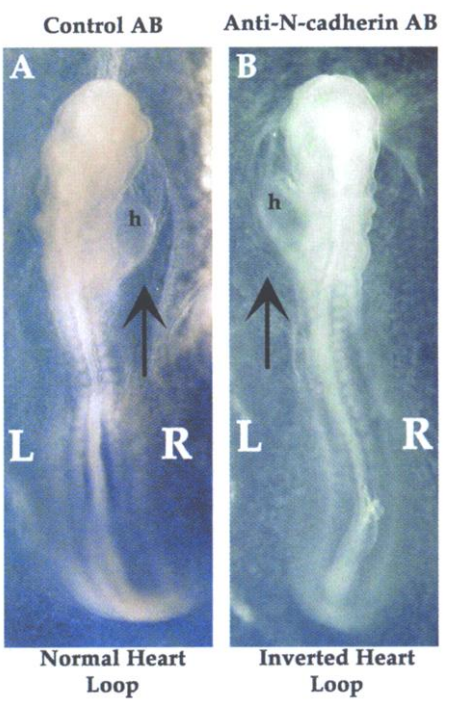

Fig. 2. Randomization of heart looping after blocking N-cadherin function. HH stage 3 embryos in New culture (*22*) were treated with 1 μl of supernatant of anti N-cadherin function-blocking antibody or 1 μl of supernatant of control antibody for 24 to 36 hours. Embryos are shown with the dorsal side up, and arrows point to the heart (h); left (L) and right (R) sides are indicated. (**A**) Most of the control antibody-treated embryos displayed normal heart looping to the right, and only 8% looped to the left (n = 25). (**B**) In contrast, 41% of embryos treated with the anti-N-cadherin function-blocking antibody displayed leftward heart looping (n = 58).

Table 1. Heart randomization after blocking N-cadherin in new culture.

Embryonic stage	Treatment	Embryos analyzed	Normal heart looping (right)	Inverted heart looping (left)	Percent inverted
St 3–4	Anti-N-cadherin (NCD-2)	58	34	24	41
St 3–4	Anti-dystroglycan	25	23	2	8
St 5	Anti-N-cadherin (NCD-2)	16	13	3	18
St 6	Anti-N-cadherin (NCD-2)	14	14	0	0

sion on the right, which suggests an inversion of the normal pattern. It is interesting to note that some of these abnormal patterns were observed even when the heart looped in the normal direction; 46% of the embryos treated with anti-N-cadherin and processed for Pitx2 expression displayed leftward heart looping (n = 14), and most of these showed clear Pitx2 expression in the left precardiac mesoderm, regardless of the direction of heart looping. Control embryos showed normal Pitx2 expression and rightward heart looping (n = 10; Fig. 4, E and F). These findings suggest that asymmetric expression of Pitx2 in the precardiac mesenchyme may not be essential for determining the direction of heart looping, even though its ectopic expression is sufficient to alter looping (*19*, *20*). Interestingly, Nodal expression was unaltered in the left side of the node and the left lateral plate mesoderm after N-cadherin function was blocked at stage 3 to 4 despite the randomization of heart looping (n = 14; control n = 4) (Fig. 4, I to L). Similarly, Lefty, a downstream target of Nodal, was unperturbed (n = 9; control n = 5).

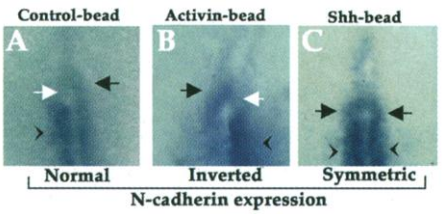

Fig. 3. N-cadherin expression pattern is modified by ectopic activin and Shh. Beads coated with activin, Shh, or BSA (control) were implanted adjacent to Hensen's node in HH stage 3 embryos (*22*). Activin beads were implanted on the left side of the node (opposite normal ActRIIa expression pattern) and Shh beads were implanted on the right side (opposite normal Shh expression pattern). Embryos were grown in New culture (*22*) for 6 to 9 hours and N-cadherin expression was detected by in situ hybridization. (**A**) Normal N-cadherin expression pattern after control bead implant. (**B**) Inverted node shape and N-cadherin expression pattern after activin treatment. (**C**) Shh treatment modified N-cadherin expression in various ways. Most embryos showed inversions similar to those generated by activin (26%), whereas 20% showed symmetric expression both in the node and in the primitive streak (shown here).

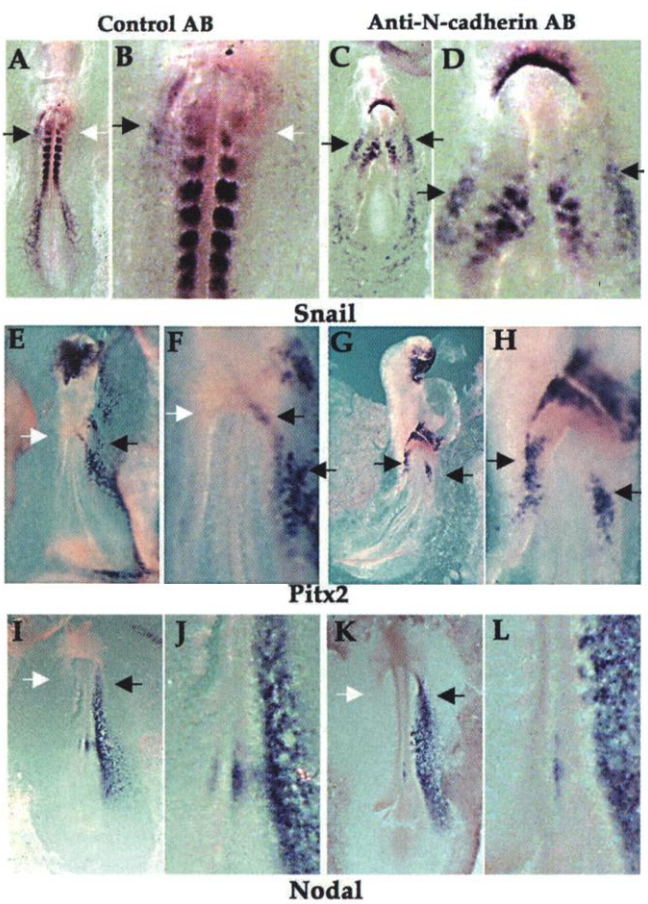

Fig. 4. Alteration of Snail and Pitx2 but not of Nodal expression patterns after blocking N-cadherin function. Stage 3 embryos were treated with anti-N-cadherin function-blocking antibody (**C**, **D**, **G**, **H**, **K**, and **L**) or control antibody (**A**, **B**, **E**, **F**, **I**, and **J**) in New culture (*22*) for 12 to 24 hours. In situ hybridization was performed on embryos of 6 to 8 somites for Snail and Nodal and on embryos of 10 to 14 somites for Pitx2. Embryos are shown with the ventral side up in consecutive pairs of low-power (A, C, E, G, I, and K) and high-power (B, D, F, H, J, and L) images. Black arrows point to areas of high expression, and white arrows point to areas of low expression. (A) Control antibody-treated embryos showed normal Snail expression in the right lateral plate mesoderm. (C) Example of anti-N-cadherin–treated embryo displaying bilateral expression of Snail. (E) Normal expression of Pitx2 in the left lateral plate mesoderm was observed in control antibody-treated embryos. (G) Anti-N-cadherin–treated embryo showing bilateral expression of Pitx2. (I) Normal expression pattern of Nodal on the left lateral plate mesoderm. (K) No effect was seen in anti-N-cadherin–treated embryos.

Our results suggest that the early function of N-cadherin may be independent of some of the known downstream effectors of left-right asymmetry expressed in the lateral plate mesoderm, particularly Nodal and Lefty. N-cadherin participation in left-right asymmetry seems to operate earlier than Nodal and to be dominant over the signal mediated by normal expression of Nodal. Therefore, it may mediate a pathway parallel to that mediated by Nodal. Thus, some of the early events in left-right asymmetry may establish two or more molecular cascades responsible for different functions leading to proper left-right morphogenesis. It is not yet clear whether cross-talk exists between these pathways. Other reports have also supported the view that parallel pathways regulate left-right asymmetry (*14*, *17*, *19*).

The asymmetric distribution of N-cadherin in gastrula-stage chicken embryos correlates with a critical period when N-cadherin function is required both for correct expression of downstream components of the left-right pathway as well as for proper left-right morphogenesis. The well-established function of N-cadherin as a homophilic cell adhesion molecule suggests a critical role during early gastrulation, when cells are moving through the node and primitive streak to segregate the three germ layers. Thus, N-cadherin is likely to act in a mechanical fashion to mediate cell-cell interactions that affect cell movements and/or behavior. There are several mechanisms whereby differential adhesion might create asymmetric patterning. One possibility is that a relative increase in cell adhesion on one side of the primitive streak and Hensen's node may delay cell movement during gastrulation in an asymmetric fashion, resulting in exposure of cells to different signals. Alternatively, adhesion forces might be required to specify cell polarity, alter motility of nodal cilia (*23*), establish a midline barrier (*19*, *39*), or be associated with cell-sorting mechanisms. The requirement for N-cadherin is transient, which suggests that a carefully timed adhesion event is necessary to determine left-right asymmetry.

References and Notes

1. M. C. Fishman and K. R. Chien, *Development* **124**, 2099 (1997).
2. V. Hensen, *Z. Anat. Entwgesch.* **1**, 353 (1876).
3. R. Wetzel, *Arch. Entwicklungsmech.* **119**, 188 (1929).
4. K. Hara, in *A Milestone of a Half Century Since Spemann*, O. Nakamura and S. Toivonen, Eds. (Elsevier/North Holland, Amsterdam, 1978), chap. 7.
5. J. Cooke, *Nature* **374**, 681 (1995).
6. N. G. Lepori, *Monit. Zool. Ital.* **3**, 33 (1969).
7. R. P. Harvey, *Cell* **94**, 273 (1998).
8. A. F. Ramsdell and H. J. Yost, *Trends Genet.* **14**, 459 (1998).
9. T. King and N. A. Brown, *Curr. Biol.* **9**, R18 (1999).
10. R. S. Beddington and E. J. Robertson, *Cell* **96**, 195 (1999).
11. H. J. Yost, *Curr. Opin. Genet. Dev.* **9**, 422 (1999).
12. S. M. Pagan-Westphal and C. J. Tabin, *Cell* **93**, 25 (1998).

13. M. Levin, R. L. Johnson, C. D. Stern, M. Kuehn, C. Tabin, *Cell* **82**, 803 (1995).
14. T. Boettger, L. Wittler, M. Kessel, *Curr. Biol.* **9**, 277 (1999).
15. Y. Yokouchi, K. J. Vogan, R. V. Pearse II, C. J. Tabin, *Cell* **98**, 573 (1999).
16. C. Rodriguez Esteban *et al.*, *Nature* **401**, 243 (1999).
17. A. Isaac, M. G. Sargent, J. Cooke, *Science* **275**, 1301 (1997).
18. M. Sefton, S. Sanchez, M. A. Nieto, *Development* **125**, 3111 (1998).
19. A. K. Ryan *et al.*, *Nature* **394**, 545 (1998).
20. M. Logan, S. M. Pagan-Westphal, D. M. Smith, L. Paganessi, C. J. Tabin, *Cell* **94**, 307 (1998).
21. H. Yoshioka *et al.*, *Cell* **94**, 299 (1998).
22. E. N. Meyers and G. R. Martin, *Science* **285**, 403 (1999).
23. S. Nonaka *et al.*, *Cell* **95**, 829 (1998).
24. D. M. Supp, D. P. Witte, S. S. Potter, M. Brueckner, *Nature* **389**, 963 (1997).
25. M. Levin and M. Mercola, *Development* **126**, 4703 (1999).
26. ———, *Dev. Biol.* **203**, 90 (1998).
27. K. Hatta, T. S. Okada, M. Takeichi, *Proc. Natl. Acad. Sci. U.S.A.* **82**, 2789 (1985).
28. K. Hatta and M. Takeichi, *Nature* **320**, 447 (1986).
29. In situ hybridization of antisense RNA probes was performed as described [A. K. Knecht, P. J. Good, I. B. Dawid, R. M. Harland, *Development* **121**, 1927 (1995); D. Henrique *et al.*, *Nature* **375**, 787 (1995)]. The full-length chicken N-cadherin (gift of M. Takeichi) was digested with Pst I, and a 461-base-pair fragment corresponding to the extracellular domain was cloned into pBS II SK+ and used to detect N-cadherin expression. Other probes were used as recommended and provided as follows: Nodal (M. R. Kuehn), Snail (A. Nieto), Lefty and Pitx2 (J. C. Izpizua-Belmonte), Shh and FGF8 (C. Tabin), and ActRIIa (C. Stern).
30. V. Hamburger and H. L. Hamilton, *J. Morphol.* **88**, 49 (1951).
31. R. L. DeHaan, *Exp. Cell. Res.* **29**, 544 (1963).
32. R. L. DeHaan, in *Organogenesis*, R. L. DeHaan and H. Ursprung, Eds. (Holt, Reinhart, Winston, New York, 1965), p. 377.
33. R. L. DeHaan, *Contrib. Embryol.* **263**, 111 (1966).
34. G. C. Rosenquist, *Dev. Biol.* **22**, 461 (1970).
35. V. Garcia-Martinez, I. S. Alvarez, G. C. Schoenwolf, *J. Exp. Zool.* **267**, 431 (1993).
36. V. Garcia-Martinez and G. C. Schoenwolf, *Dev. Biol.* **159**, 706 (1993).
37. White Leghorn chicken embryos were staged according to Hamburger and Hamilton (*30*). Antibodies were used as follows: 1 μl of saturated hybridoma supernatant of monoclonal antibody NCD-2, anti-N-cadherin, or control antibody IIH6C4 (chosen as a control because it recognizes an extracellular epitope present in both the primitive streak and the node of stage 4 to 6 chicken embryos) was applied from above to the ventral side of the node in embryos prepared for New culture according to [D. A. T. New, *J. Embryol. Exp. Morphol.* **3**, 320 (1955)]. Affi-Gel beads (Bio-Rad) were rinsed three times in large volumes of phosphate-buffered saline (PBS) and incubated for 1 hour at room temperature in 0.1% BSA in PBS solution (control) or with activin (R&D Systems; 10 units/μl) or Shh (from E. Turner; 4 μg/μl) and rinsed briefly before implantation between the epiblast and endoderm. These dosages of activin and Shh were sufficient to randomize the direction of heart looping in our hands.
38. K. K. Linask, K. A. Knudsen, Y. H. Gui, *Dev. Biol.* **185**, 148 (1997); S. Nakagawa and M. Takeichi, *Dev. Growth Differ.* **39**, 451 (1997).
39. C. Meno *et al.*, *Cell* **94**, 287 (1998).
40. Supported by U.S. Public Health Service grant HD 15527 (M.B.-F.), American Heart Association 1140-FI1 (M.I.G-C.), and the Summer Undergraduate Research Fellowship, Caltech (E.V.). We thank C. Baker, A. Groves, C. LaBonne, and B. E. Murray for helpful discussions and comments and R. Velasco for help with sectioning.

11 November 1999; accepted 5 April 2000

REPORTS

Influenza B Virus in Seals

A. D. M. E. Osterhaus,[1,2,*] G. F. Rimmelzwaan,[1] B. E. E. Martina,[2] T. M. Bestebroer,[1] R. A. M. Fouchier[1]

Influenza B virus is a human pathogen whose origin and possible reservoir in nature are not known. An influenza B virus was isolated from a naturally infected harbor seal (*Phoca vitulina*) and was found to be infectious to seal kidney cells in vitro. Sequence analyses and serology indicated that influenza virus B/Seal/Netherlands/1/99 is closely related to strains that circulated in humans 4 to 5 years earlier. Retrospective analyses of sera collected from 971 seals showed a prevalence of antibodies to influenza B virus in 2% of the animals after 1995 and in none before 1995. This animal reservoir, harboring influenza B viruses that have circulated in the past, may pose a direct threat to humans.

Influenza A, B, and C viruses cause influenza in humans (*1*). Influenza A viruses have been isolated from many species, and aquatic birds may form the natural reservoir from which pandemics and subsequent epidemics in humans have originated (*2*). In contrast, influenza C virus has been isolated from humans and pigs, and influenza B virus infection is supposed to be restricted to humans. Previous reports of influenza B virus infection of a dog and a pig did not meet the established criteria to prove infection (*3, 4*). The origins and possible natural reservoirs of influenza B and C viruses, as well as their potential to infect other species, are unknown (*1*).

Herpes-, morbili-, calici-, and poxviruses have been identified as causes of significant morbidity and mortality among pinniped species (*5–11*). In addition, influenza A viruses of avian origin, including four different antigenic subtypes (H3N3, H4N5, H4N6, and H7N7), have caused outbreaks of influenza among seals (*12–15*).

Seals stranded on the Dutch coast are admitted to the Seal Rehabilitation and Research Center (SRRC) in Pieterburen, the Netherlands, for rehabilitation. In the spring of 1999, 12 juvenile harbor seals with respiratory problems, but not infected with phocine herpesvirus (PHV) or phocine distemper virus (PDV), were tested for influenza virus infection. Cytopathic changes were noted within 3 days of inoculation of a throat swab sample from an 8-month-old animal (seal 99-012) in Madine Darby canine kidney (MDCK) cells (*16*). The supernatant of this cell culture agglutinated turkey erythrocytes in a hemagglutination (HAI) assay (*16*). Negative contrast electron microscopic analysis of the hemagglutinin (HA)–positive culture supernatant showed the presence of orthomyxovirus-like particles (*17*). To our surprise, the presence of influenza B virus was identified by reverse transcription polymerase chain reaction (RT-PCR) analysis of RNA isolated from the culture supernatant (*18*). A semi-quantitative RT-PCR performed with the original throat swab obtained from seal 99-012 confirmed the presence of influenza B virus at levels equivalent to approximately 400 50% tissue culture infectious dosis ($TCID_{50}$) of virus, present in the supernatant of MDCK cell culture infected with influenza B virus (Fig. 1). This influenza virus, B/Seal/Netherlands/1/99, could be propagated in primary seal kidney cell cultures (*7, 19*).

To exclude sample contamination in the laboratory, serum samples collected from seal 99-012 before and after virus isolation were tested for the presence of antibodies that inhibit hemagglutination (HAI) (*20*) of B/Seal/Netherlands/1/99. Samples collected 44 days before and at the day of virus isolation were negative (HAI titer <6), whereas the sample collected 83 days after virus isolation showed a HAI titer of 192, confirming that seal 99-012 had been infected with influenza B virus. Sera from seven other juvenile harbor seals, kept in the same basin as seal 99-012, were also tested for the presence of HAI. The serum of one seal, 99-041, collected 61 days after the day of virus isolation from seal 99-012, showed a HAI titer of 48. All the other sera from this and the other animals were negative (HAI titer <6). We were unable to detect influenza B virus by RT-PCR in the throat swabs collected from seal 99-041 at 34 days before and 61 days after virus isolation from seal 99-012 (*17*).

Quantitative analyses of immunoglobulin G (IgG) antibodies to nucleoprotein (NP) (*17*) and envelope glycoproteins HA and neuraminidase (HA/NA) of influenza B virus, as well as IgM antibodies to NP as an indicator for primary infection, were performed by enzyme-linked immunosorbent assay (ELISA) (*20, 21*) (Fig. 2). In seals 99-012 and 99-041, IgG antibodies to HA/NA and NP were detected, which increased over time and correlated with virus-neutralizing and HAI antibodies (*17*). Both harbor seals displayed decreasing levels of IgM antibody to

[1]National Influenza Center, Department of Virology, Erasmus University, Doctor Molewaterplein 50, 3015 GE Rotterdam, Netherlands. [2]Seal Rehabilitation and Research Center, Hoofdstraat 94a, 9968 AG Pieterburen, Netherlands.

*To whom correspondence should be addressed. E-mail: osterhaus@viro.fgg.eur.nl